*NDT*
Journal of Non-Destructive Testing

MDPI

*Article*

# Integrated GPR and Electrochemical Methods for Monitoring Steel Rebar Corrosion in Reinforced Structure

**Enzo Rizzo [1,*], Federica Zanotto [2], Giacomo Fornasari [1], Sofia Rando [2], Francesca Gallo [2], Andrea Balbo [2] and Vincenzo Grassi [2]**

[1] Department of Physics and Earth Sciences, University of Ferrara, Via G. Saragat 1, 44122 Ferrara, Italy; giacomo.fornasari@unife.it
[2] Department of Engineering, Corrosion and Metallurgy Study Centre "A. Daccò", University of Ferrara, Via G. Saragat 4A, 44122 Ferrara, Italy; federica.zanotto@unife.it (F.Z.); sofia.rando@unife.it (S.R.); francesca.gallo@unife.it (F.G.); andrea.balbo@unife.it (A.B.); vincenzo.grassi@unife.it (V.G.)
* Correspondence: enzo.rizzo@unife.it

**Abstract**

Reinforced concrete structures, once considered very durable and capable of withstanding a variety of adverse environmental conditions, often suffer from premature reinforcement corrosion, compromising their safety and serviceability. Ensuring the safety of bridges and buildings requires effective, non-destructive inspection and monitoring techniques to assess the state of degradation without damaging the integrity of the asset. Although a wide range of non-destructive testing (NDT) methods is currently available, few are capable of identifying durability issues during the initial stages before the damage becomes critical. To address this gap, this paper describes an innovative laboratory experiment based on an integrated approach that combines Ground-Penetrating Radar (GPR) and electrochemical methods. This research represents an advanced step in our ongoing projects, merging geophysical and electrochemical expertise to enhance diagnostic precision. A reinforced cement mortar specimen was subjected to free corrosion via partial immersion in sodium chloride solutions of varying concentrations (1, 10, and 35 g/L), followed by an accelerated corrosion phase. The phenomenon was monitored simultaneously using GPR and electrochemical tests. Each technique provided specific information, but a data integration method used in the operating system will further improve the overall quality of diagnosis. Specifically, the application of the Hilbert Transform to GPR signals allowed for a correlation between envelope amplitude variations and the electrochemical behavior of the rebars. These laboratory results highlighted that an integrated observation was useful to indirectly observe the evolution of the phenomenon of corrosion in the steel reinforcement embedded in the mortar specimens.

**Keywords:** rebar corrosion monitoring; reinforced concrete; non-destructive testing (NDT); ground-penetrating radar (GPR); electrochemical monitoring

Check for updates

Academic Editor: Siqi Wang

Received: 15 April 2026
Revised: 14 May 2026
Accepted: 21 May 2026
Published: 25 May 2026

**Copyright:** © 2026 by the authors. Licensee MDPI, Basel, Switzerland. This article is an open access article distributed under the terms and conditions of the Creative Commons Attribution (CC BY) license.

## 1. Introduction

Cement-based materials, which are fundamental for building and civil infrastructure, are susceptible to various forms of deterioration. These include mechanical degradation, caused by stresses such as impact, erosion, and structural overload; physical degradation, attributable to freeze–thaw cycles and thermal fluctuations; and chemical degradation, which includes alkali–silica reaction, sulfate attack, steel corrosion, and physico-chemical changes resulting from exposure to elevated temperatures [1,2]. This phenomenon results

in significant economic losses [3], reduces the service life and durability of infrastructure, and can potentially compromise public safety. In reinforced concrete structures, the high alkalinity of the pore solution (pH 12–13) promotes the formation of a thin passivating layer on the steel rebars, significantly reducing the corrosion rate. However, when the pH of the concrete drops below a critical level or the chloride concentration exceeds a specific threshold, this protective layer becomes unstable, leading to the depassivation of the steel [1–8]. The instability and subsequent breakdown of the passive film cause corrosion initiation and propagation in steel. The corrosion products formed during the oxidation process occupy a significantly larger volume than the original metal [9]. This volumetric expansion around the reinforcement induces internal stresses that result in micro-cracks and voids within the concrete cover [10]. These defects increase the permeability of the concrete, thereby accelerating the ingress of moisture and aggressive agents. Neglecting this process can result in serious concrete damage, which typically leads to further deterioration of the reinforced concrete (RC) structural elements [1,2]. By the time the first cracks become visible on the concrete surface, rebar corrosion has generally reached an advanced stage, necessitating extensive maintenance [9,11]. Consequently, a reliable inspection method is essential at an early stage before the structural integrity of the RC structure is seriously compromised [12–14]. Early detection of rebar corrosion in bridges, tunnels, buildings, and other RC structures is crucial for minimizing repair costs, optimizing maintenance scheduling, and developing effective monitoring strategies. These plans provide insights into the structural health of the structures under investigation. One of the most promising approaches to delay the degradation of existing structures is the extensive use of Non-Destructive Techniques (NDTs) [15]. These methods are becoming very important in civil engineering for the continuous characterization and monitoring of complex reinforced concrete elements, like bridges and tunnels; however, NDT methods still have some limitations to overcome [15–21]. Based on the analyses of physical property variations, and characterized by high resolution and repeatability, these techniques enable the identification of defects and fractures resulting from induced stresses, intrinsic inhomogeneities, or structural issues. In this perspective, the recent advancements in NDT data visualization are expected to further promote the adoption of advanced NDT methods in the future [21–24]. The integration of multiple NDTs is essential to overcome the limitations of instantaneous corrosion rate measurements obtained with electrochemical techniques and to improve the service life prediction of RC structures.

Over the last decade, several studies have employed Ground-Penetrating Radar (GPR) to monitor rebar corrosion under laboratory conditions [11,12,16–19,21,22]. Since the corrosion of RC is a slow process, and it takes a long time to progress, many of these studies have adopted accelerated corrosion methods [11,14,18,21–23,25–27]. Some researchers reported low amplitude variation in GPR signals at the end of experiments [17,28,29], whereas others found high amplitude variations [18,29,30]. All these studies on the use of GPR aimed at a qualitative detection of the corrosion phenomena in steel reinforcements. For these reasons, it is still fundamental to clarify the influence of the corrosion process on the GPR signal with accurate laboratory tests. While previous research has focused on the qualitative detection of corrosion, this study aims to fill the gap laying the groundwork for the development of a quantitative correlation between GPR signal variations and reinforcement mass loss, utilizing a multi-sensor approach to validate the findings.

Following two previous studies on rebar corrosion monitoring using GPR [16,21], this work presents a GPR experiment conducted on two new samples and integrated with careful electrochemical measurements. In detail, the experimental program involved monitoring two specimens: Slab-A, exposed to demineralized water, and Slab-B, partially immersed in a sodium chloride solution of increasing concentration. Upon completion of

the free corrosion period, the latter was subjected to accelerated corrosion. GPR spectra were elaborated upon, taking into account a mathematical envelope filter (Hilbert Transform). During the exposure, electrochemical measurements were performed. A Saturated Calomel Electrode (SCE) was placed at specific points on the concrete surface to measure the corrosion potential ($E_{cor}$) of the rebar. The spontaneous potential (SP) of steel reinforcements measured on the surface of concrete is one of the earliest methods for assessing the corrosion condition of RC [30,31]. This method has been adopted as the standard in several countries [32,33]. Additionally, the instantaneous corrosion rate of the reinforcing steel was determined using Linear Polarization Resistance (LPR) [34].

## 2. Materials and Methods

### 2.1. Sample Preparation

The specimens were cast using 32.5 R cement and sand. As an initial approach, to simplify the specimen's preparation, reinforced cement mortar was used instead of concrete. Figure 1a shows a sketch of the steel-reinforced mortar specimen with the following dimensions: length (l) = 500 mm, width (w) = 300 mm, and height (h) = 80 mm. The specimens were cast with a central ribbed rebar (steel B450C), having a 10 mm diameter and a length of 350 mm. An electrical cupper cable was fixed to the rebar, as shown in Figure 1b, in order to connect it to a DC power supply during the electrochemical measurements. The electrical connection was protected using heat-shrink tubing. The rebar was painted with epoxy resin, leaving an exposed area of approximately 25 $cm^2$ (corresponding to a rebar length of 8 cm) in the center of the rebar (Figure 1c). A wooden formwork was used to cast the reinforced mortar specimens (Figure 1c).

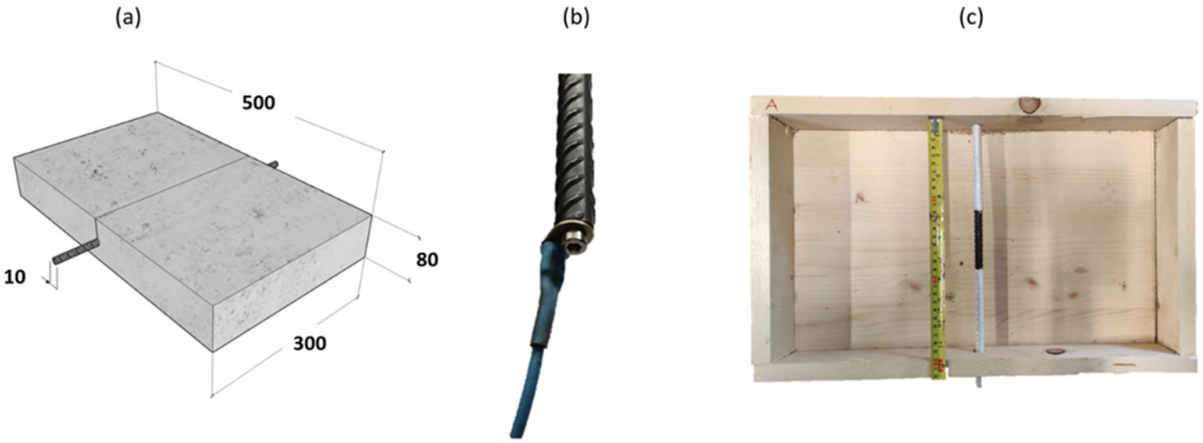



**Figure 1.** (**a**) Sketch of the reinforced cement mortar specimen; (**b**) electrical connection to the steel rebar; and (**c**) wooden formwork and steel rebar used to cast the reinforced cement mortar specimens.

The rebar was positioned within the wooden formwork, and the cement mortar was cast, providing a mortar cover of 30 mm at the top and 40 mm at the bottom. After 30 days of curing, the wooden formwork was removed, and the reinforced mortar slab was ready for the corrosion tests (Figure 2). Before exposure to the test solutions, the specimens were coated with epoxy resin on the four lateral faces (Figure 2a) and on the bottom surface, except for an 8 cm × 10 cm window, which was left uncovered (Figure 2b). This configuration was designed to ensure that chloride penetration occurred exclusively through the central portion of the lower surface.

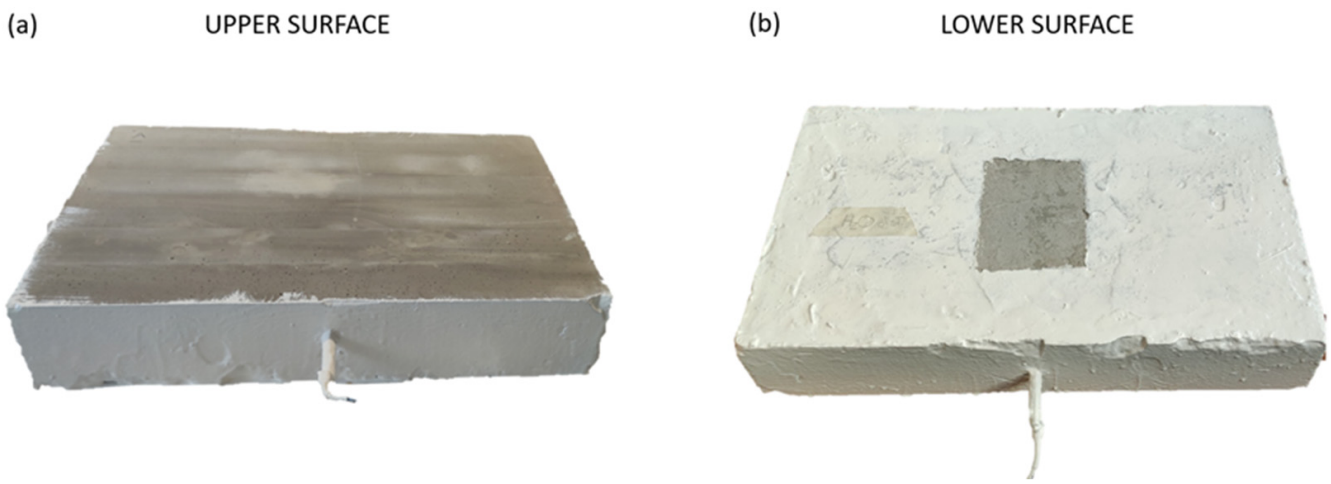



**Figure 2.** Upper (**a**) and lower (**b**) surfaces of the final reinforced mortar specimen.

### 2.2. Exposure Conditions

The study was conducted on two specimens simultaneously: Slab-A, which was exposed to deionized water throughout the test period and was used as reference, and Slab-B, which was exposed to sodium chloride solutions at increasing concentrations of NaCl. Slab-B was initially monitored under natural corrosion ("free corrosion") conditions, followed by accelerated corrosion (induced corrosion obtained by applying an external current). Each slab was placed in a shallow tank for partial immersion, maintaining a constant depth of 1.0 cm from the bottom to prevent the exposed ends of the rebar from coming into contact with the solution. The water level was kept constant during the whole investigation period by refilling with water. The exposure period of the mortar slabs was divided into different phases (Table 1):

- Phase 1: Slab-A was partially immersed in deionized water (this condition was considered the reference).
- Phase 2: Slab-B was immersed in 1 g/L NaCl solution in free corrosion conditions for 7 days.
- Phase 3: Sodium chloride concentration in test solution of Slab-B was increased to 10 g/L NaCl (still in free corrosion condition) and then maintained for 7 days.
- Phase 4: Sodium chloride concentration in test solution of Slab-B was increased to 35 g/L NaCl (still in free corrosion condition) and then maintained for 7 days.
- Phase 5: Steel rebar in Slab-B was subjected to accelerated corrosion in the 35 g/L NaCl solution for 15 days.

**Table 1.** $E_{cor}$ measurements for Slab-A and Slab-B across all experimental phases.

| **Specimens** | **Slab-A** | **Slab-B** | | | |
|---|---|---|---|---|---|
| Test conditions | Deionized water | Free (or natural) corrosion | | | Accelerated corrosion |
| Phase No. | Phase 1 | Phase 2 | Phase 3 | Phase 4 | Phase 5 |
| NaCl % | / | 1 g/L | 10 g/L | 35 g/L | 35 g/L |
| $E_{cor}$ measurements No. | 18 | 10 | 3 | 2 | 3 |
| Experimental days | 18 | 10 | 7 | 7 | 15 |

### 2.3. Electrochemical Tests

To monitor the passivity or corrosion state of the reinforcing bars in both specimens throughout the exposure period, corrosion potential values ($E_{cor}$) were acquired versus an external Saturated Calomel Electrode (SCE). The $E_{cor}$ measurements were carried on in the correspondence of specific positions. These positions were established by covering the entire surface of the sample with a predetermined mesh of 54 points on a grid using a wooden table. This setup ensured that the reference electrode was placed at the same investigation points throughout the study (Figure 3). The SCE reference electrode was placed on a wet cloth, positioned between the slab's surface and the wooden table to ensure electrolytic contact, and it was connected to a high impedance multivoltmeter. The positive pole was connected to the rebar, thus acting as working electrode.

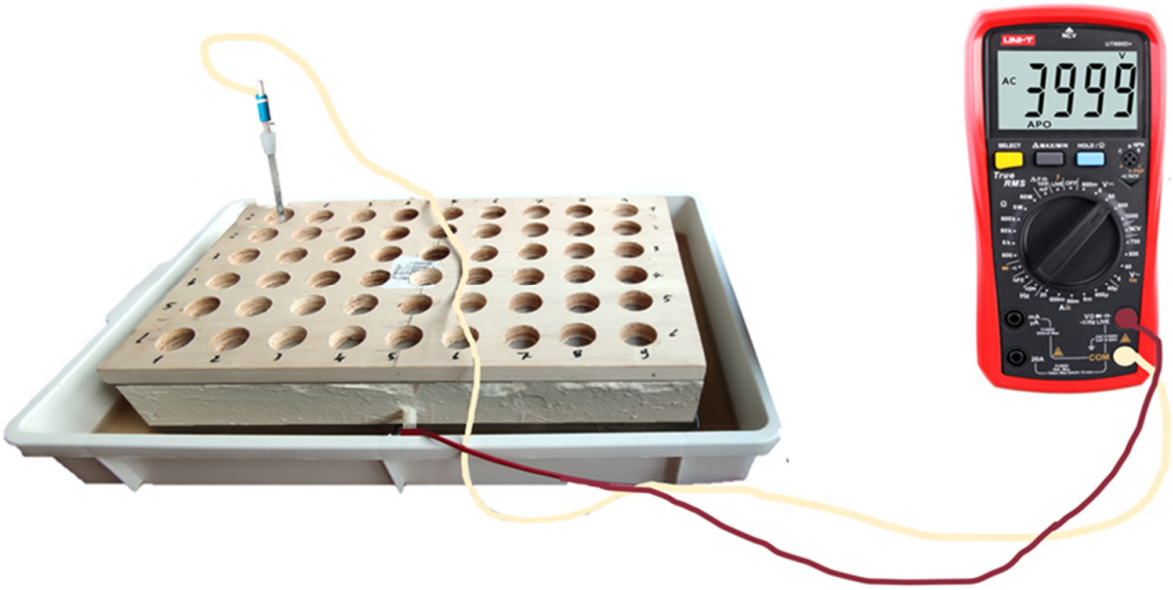



**Figure 3.** Acquisitions of corrosion potentials $E_{cor}$ vs. SCE on the steel-reinforced mortar specimens' surface. The red and yellow electrical cables are connected to the reference electrode (Saturated Calomel Electrode) and the rebar, respectively.

The $E_{cor}$ monitoring was conducted on Slab-A for 18 days in deionized water and on Slab-B in free corrosion at various NaCl concentrations, as described in Table 1.

The polarization resistance ($R_p$) values were determined potentiostatically (by LPR) applying an anodic polarization of +10 mV vs. $E_{cor}$ for 300 s and by dividing this anodic polarization by the stable anodic current measured. Finally, from $R_p$, $I_{cor}$ values were determined by means of the constant B in the equation

$$I_{cor} = B/R_p, \quad (1)$$

proposed by Stern [35]. The Stern–Geary constant (B) was assumed to be 52 mV for steel in the passive state and 26 mV for the active or corroded state. However, a value of 26 mV can be applied across all conditions, as a twofold error in the passive state is typically considered negligible in practice [36].

During phase 5, the accelerated corrosion test was conducted on Slab-B. The positive terminal of a DC power supply (OK320-KA3005D by RND LAB company, Manchester, UK) was connected to the steel rebar (anode), while the negative terminal was connected to a stainless-steel mesh (cathode) immersed in a 35 g/L NaCl solution (Figure 4). Through the DC power supply, we established a constant corrosion current of 0.025 A (corresponding to a current density of about 1 mA/cm$^2$) for 10 days, which was increased

to 0.050 A (corresponding to a current density of about 2 mA/cm$^2$) for five days further. The DC power supply automatically adjusts the voltage to maintain the current constant for all days of the investigation. The DC power supply was switched off during $E_{cor}$ and GPR acquisitions.

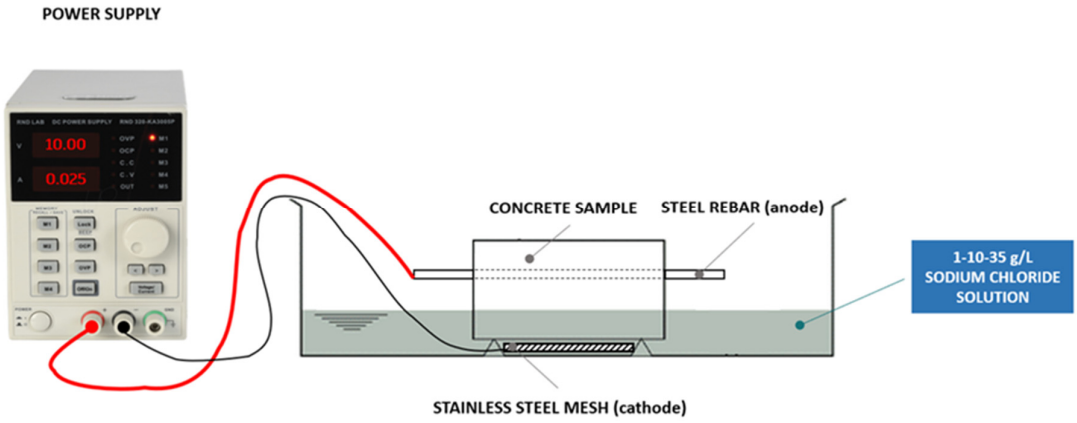



**Figure 4.** Sketch of the accelerated corrosion test conducted on Slab-B partially immersed in a 35 g/L NaCl solution.

At the end of the accelerated corrosion test, the reinforcement bar was extracted from the mortar sample. The exposed 8 cm portion (previously left uncoated by epoxy resin) was cut and cleaned from the corrosion products through a chemical pickling process. The actual mass loss at the end of the accelerated corrosion was determined by knowing the initial weight of the rebar (and proportionally determining the weight of the exposed 8 cm portion).

### *2.4. GPR Acquisitions*

GPR scans were performed throughout all experimental phases. The antenna used (a 2 GHz GPR C-Thrue) has dimensions of 285 × 200 × 160 mm (L × W × H). To ensure full coverage of the investigated area, a Plexiglass support base was fabricated to increase the surface on which to move the antenna. A grid consisting of 30 reference lines, spaced 10 mm apart, was marked on the Plexiglass base across the entire width of the mortar specimen. These lines guided the GPR scans to ensure spatial consistency and repeatability of the radargrams across all experimental phases. GPR data were collected with an inter-scan spacing of 10 mm, resulting in 30 radargrams per scan. To maintain a constant profile length of 500 mm, physical stoppers were installed at the start and end of the Plexiglass base. This setup ensured that the antenna followed a consistent path, providing reproducible start and end points for every acquisition. GPR acquisitions started at the lower edge of the specimen, following the first reference line on the Plexiglass base (Position 1, Figure 5). The first radargram was acquired with the antenna at Position 2 (Figure 5). The survey concluded with the thirtieth radargram at the opposite edge, covering the entire 300 mm width of the sample. This final scan began at Position 3 and ended at Position 4 (Figure 5). In each phase, 34 GPR surveys were performed on Slab-B under various conditions. The schedule of these acquisitions is detailed in Table 2.

Each GPR survey consisted of 30 collected radargrams, resulting in a total of 870 radargrams across the study. Furthermore, each radargram consisted of 400 A-scans, with a trace interval of 1.25 mm and a sampling depth of 512 samples per trace. For the data processing stage, the A-scans (traces) corresponding to the rebar location were extracted from each radargram.

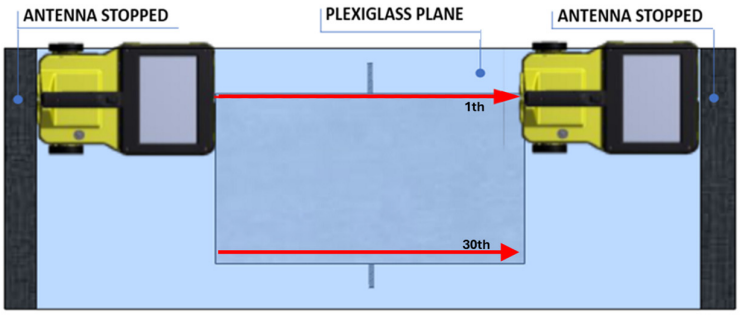



**Figure 5.** GPR acquisition system. A Plexiglass guide was placed between the slabs and the instrument to standardize radargram length and positioning. N.30 radargrams were performed for each GPR survey.

The rebar embedded in the slabs is located at 0.03 m (S) from the surface, and the corresponding Two-Way Travel time (T.W.T.) was measured at 0.6 ns (Figure 6). Therefore, the V*em* was estimated at 0.10 m/ns, taking into account the following equations:

$$Vem = S/t = S/(TWT/2), \quad (2)$$

$$Vem = C/\sqrt{\varepsilon}, \quad (3)$$

where C is the speed of light in the vacuum (0.30 m/ns).

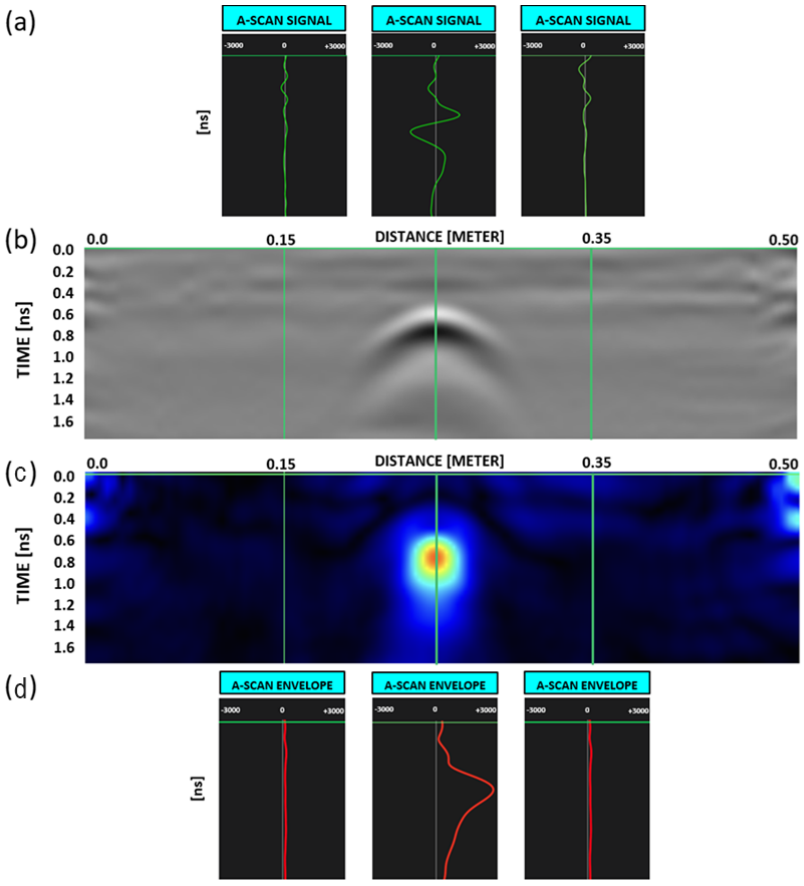



**Figure 6.** An example of radargram acquired along the slab. (**a**) A-scan traces recorded 10 cm before, exactly on, and 10 cm after the steel rebar. (**b**) Processed radargram highlighting the hyperbola due to rebar; (**c**) the envelope section after a Hilbert Transform; and (**d**) the envelope traces at 10 cm before, exactly on, and 10 cm after the steel rebar.

**Table 2.** GPR surveys on Slab-A and Slab-B across all experimental phases.

| Specimens | Slab-A | Slab-B | | | |
|---|---|---|---|---|---|
| Test Conditions | Deionized water | Free (or natural) corrosion | | | Accelerated corrosion |
| Phase No. | Phase 1 | Phase 2 | Phase 3 | Phase 4 | Phase 5 |
| NaCl % | / | 1 g/L | 10 g/L | 35 g/L | 35 g/L |
| GPR surveys | 13 | 7 | 3 | 2 | 9 |
| Experimental days | 18 | 10 | 7 | 7 | 15 |

## 3. Results

### 3.1. GPR Results

The acquired GPR dataset was processed using standard approaches Reflex-W [37], specifically applying the Hilbert Transform to calculate the signal envelope. This process considers the positive and negative components of the signal and collapses them into a single envelope that represents the instantaneous amplitude of the reflection event. Traces extracted from the top of the rebar reflections were used to monitor changes in the envelope signal at the rebar interface. These variations were then correlated with the progression of the corrosion process.

Figure 6c highlights the peak of the envelope signal for the A-scan extracted from radargram No. 15. This scan was acquired at the mid-section of Slab-A, directly above the rebar. Figure 7 illustrates the evolution of the envelope signal over 13 days of partial immersion in deionized water. The envelope values exhibit fluctuations ranging from a maximum of 3820, during the initial days of acquisition, to a minimum value of 3320 recorded at the end of the survey period. GPR acquisitions on Slab-B were conducted under two different corrosion conditions: free (natural) corrosion (using NaCl concentrations of 1, 10, and 35 g/L) and accelerated corrosion (with 35 g/L of NaCl, induced by an external DC power supply).

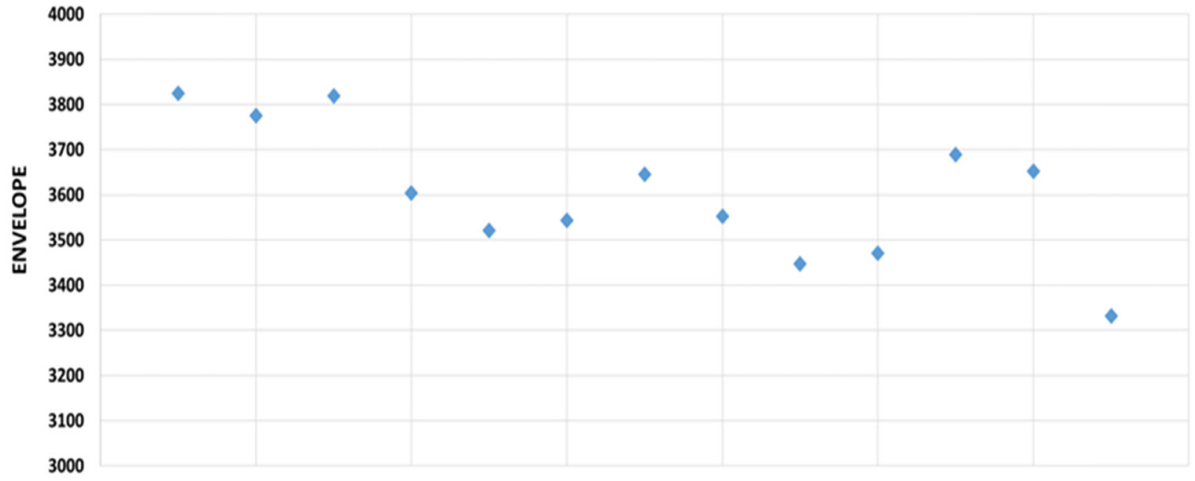



**Figure 7.** Envelope values trend for Slab-A partially immersed in deionized water during Phase 1.

During the natural corrosion phase (Figure 8) at 1 g/L NaCl concentration, the envelope signal started at 3220 and slightly increased to 3241 on the last days (Day 13). This slight upward trend resulted in an overall average value of 3223 for this specific stage.

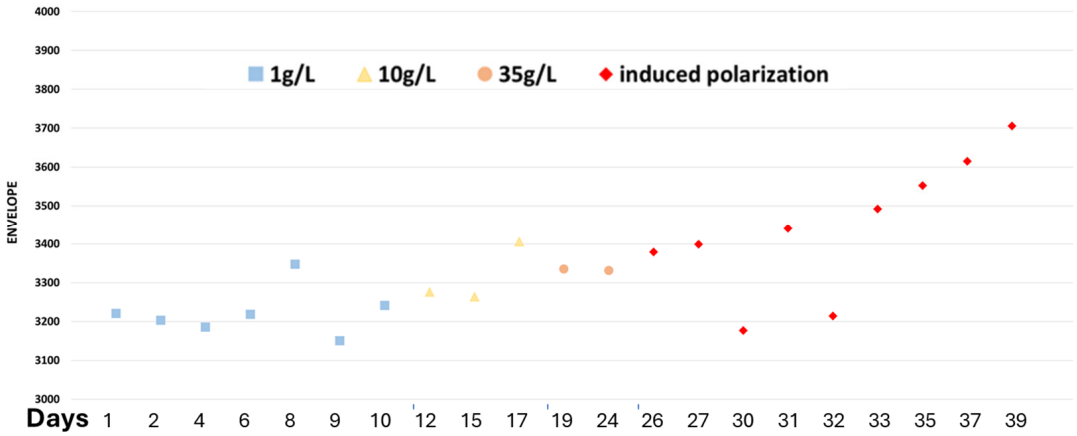



**Figure 8.** Envelope values trend for Slab-B during free corrosion phase (Phases 2, 3 and 4) and during accelerated corrosion phase (Phase 5).

During Phase 3, at a chloride concentration of 10 g/L, the first two acquisitions showed a constant envelope value of 3276 (Days 12 and 15 in Figure 9). Subsequently, an increase to 3400 was observed at the end of the phase on Day 17. The two surveys conducted during Phase 4, where the chloride concentration was further increased, exhibited stable envelope values (averaging 3335). This represents a slight increase compared to the mean value recorded in the previous stage. In summary, a gradual increase in envelope values was observed during the spontaneous corrosion stages (Phases 2, 3, and 4), rising from 3220 to 3335. Following the free corrosion phase (Day 25), accelerated corrosion was initiated by applying a constant current of 0.025 A (Phase 5). Regarding the Phase 5 data, envelope values rose from 3335 to 3379 after only one day of accelerated testing (Day 26). The signal continued to trend upward throughout this phase, except for two surveys on Days 30 and 32, which exhibited significantly lower values. During these two GPR acquisitions, the sample surface was noticeably saturated by water; consequently, it is possible that the amplitude of the electromagnetic signals decreased due to the different dielectric behavior of water. Overall, Figure 8 highlights a progressive increase in envelope values as the corrosion of the reinforcing bar advances, rising from an initial value of 3379 to 3706 after 429 h, at the conclusion of the test (Day 39).

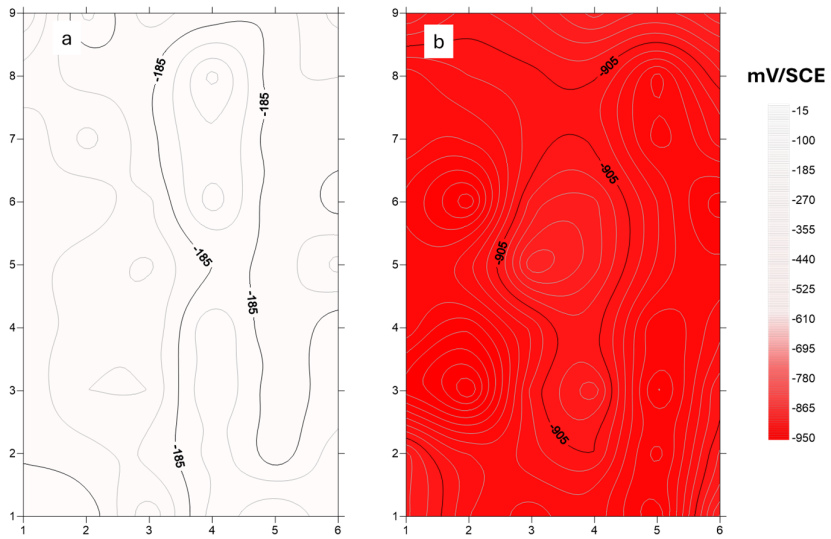



**Figure 9.** Potential values ($E_{cor}$ in mV/SCE) acquired during Phase 1 on the surface of Slab-A (**a**) and at the end of Phase 5 on Slab-B (**b**).

### 3.2. Electrochemical Results

#### 3.2.1. Corrosion Potential ($E_{cor}$) Measurements

$E_{cor}$ values were acquired on both slabs following a grid setting with 24 positions (Figure 3). Figure 9 highlights the $E_{cor}$ map obtained with a kriging contouring approach on the 24 dataset during Phase 1 on Slab-A and after some days into Phase 5 on Slab-B. To monitor the corrosion process through potential measurements, $E_{cor}$ average values over time are presented for Slab-A (Figure 10) and Slab-B (Figure 11). These values were obtained from measurements taken at two distinct positions on each specimen, in correspondence with the exposed (not covered by the epoxy resin) portion of the rebar, where the ohmic drop is expected to be lower.

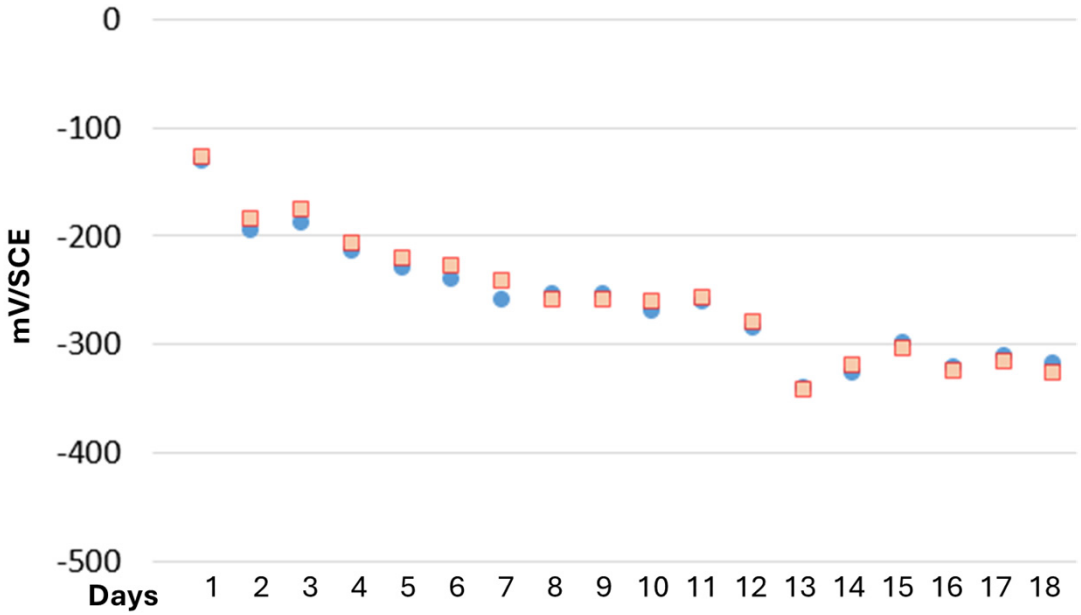



**Figure 10.** Potential values vs. days ($E_{cor}$ in mV/SCE) acquired on the surface of Slab-A during Phase 1.

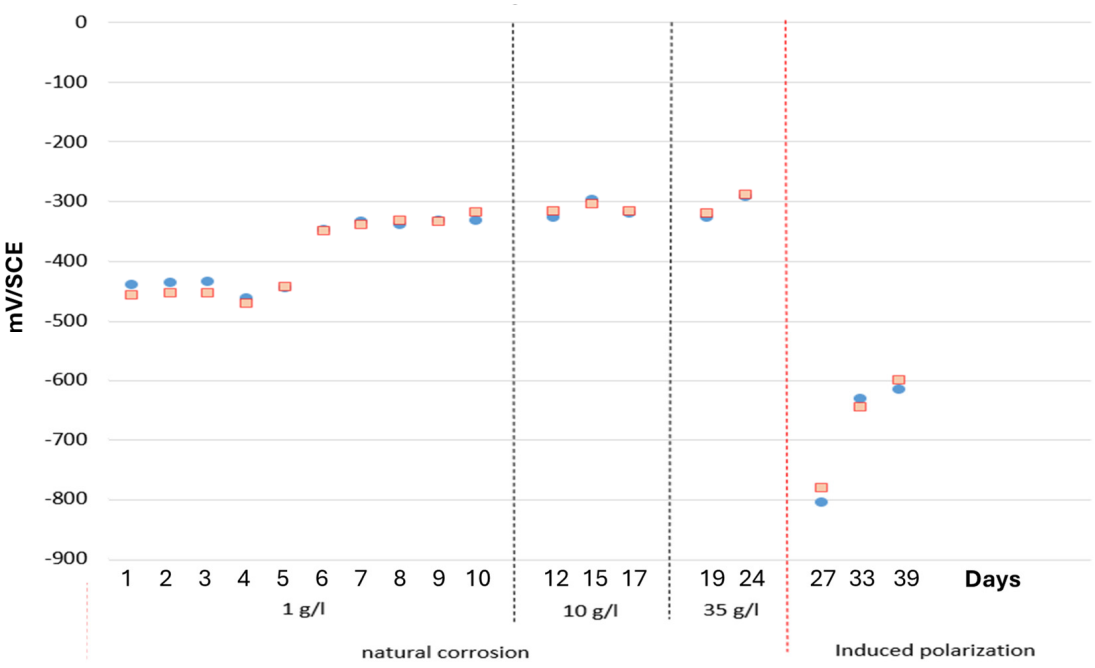



**Figure 11.** Potential values vs. days ($E_{cor}$ in mV/SCE) acquired on the surface of Slab-B during Phases 2, 3, 4, and 5 described in Table 1.

The monitored potential values exhibit a consistent trend over time across all experimental conditions. For Slab-A, the open-circuit potential (spontaneous potential) started with an average $E_{cor}$ of −129 mV/SCE. These values consistently decreased, reaching more negative potentials by the final days of the investigation in deionized water (−327 mV/SCE after 18 days). During this phase, the deionized water rose through capillary suction into the concrete pores. The pH of the pore solution decreased due to the carbonation process. Specifically, portlandite $Ca(OH)_2$ reacted with the dissolved $CO_2$ in water, leading to a decrease in pH in the pore solution. The solution's conductivity, measured with a conductometer, increased from an initial value of 240 µS/cm during the early surveys to 412 µS/cm by the end of the investigation in deionized water. This increase in electrical conductivity may be attributed to the formation of calcium bicarbonate. According to the current regulations, the initial potential values (−129 mV/SCE) reflect a passive state of the reinforcement bar, indicating the absence of active corrosion. The final value of −327 mV/SCE falls within the range defined by regulations as typical for rebar corrosion in wet, carbonated concrete [38].

Slab-B was partially immersed in a solution containing 1 g/L of NaCl. $E_{cor}$ was not measured before the immersion due to the high resistivity of the dry mortar; however, after only 24 h of specimen immersion, an average value of −447 mV/SCE was recorded. This potential value indicates active corrosion of the rebar, attributed to the rapid diffusion of chlorides through the mortar cover. Average $E_{cor}$ values fluctuated between −500 to −400 mV/SCE for six days before shifting toward more positive values, stabilizing around −318 mV/SCE until the end of Phase 2 (10 days). The corrosion potential is influenced not only by chloride ion concentration, but also by environmental factors, such as pore solution pH and oxygen availability. Once the critical chloride concentration was reached and active corrosion was initiated, the quick drop in $E_{cor}$ was measured. However, during the exposure, the environment around the rebar may change due to corrosion-product formation and carbonation. The latter, in particular, leads to a reduction in the pore solution pH and an increase in concrete porosity. Higher porosity facilitates oxygen diffusion, likely raising the oxygen-limiting current density, which results in a shift toward more positive corrosion potentials [33,39]. The potential values remained relatively stable, around −300 mV, even when the chloride concentration was increased to 10 g/L (Phase 3) and subsequently to 35 g/L (Phase 4). This suggests that the potential values stabilized because the system reached a steady-state corrosion condition, characterized by a constant reaction rate.

Average $E_{cor}$ values were also acquired during the accelerated corrosion test (polarization was suspended during potential measurements) at 48 h (Day 27), 192 h (Day 33), and 360 h (Day 39) from the beginning of the induced corrosion (Phase 5). $E_{cor}$ reached a very negative value (−780 mV/SCE) after 48 h, then it became more positive (close to −600 mV/SCE) after 192 and 360 h. Although these potential values were acquired in the absence of polarization, the system had not yet reached equilibrium; therefore, they differ significantly from the values measured under free corrosion conditions. It is possible that the formation of a thick layer of corrosion products, induced by relatively high current densities (1–2 mA/cm$^2$), limits oxygen diffusion toward the rebar surface, thereby shifting the open-circuit potential toward more negative values. It should be noted that the corrosion products generated under these conditions differ from those formed during natural processes [40]. However, the primary objective of this research was to rapidly produce a corrosion layer significant enough to demonstrate a measurable impact on the GPR envelope parameters.

3.2.2. Polarization Resistance ($R_p$) Measurements

To avoid interference caused by the accumulation of voluminous corrosion products on the reinforcing bar surface, an internal reference electrode [41] embedded in the mortar was not included in the samples. Consequently, polarization resistance, $R_p$, measurement using the linear polarization method was performed by immersing the reference electrode in the test solution at one side of the sample, relatively distant from the exposed portion of the rebar. For this reason, $R_p$ measurements may be significantly affected by ohmic drop and can be considered as apparent $R_p$ values [42]. Nevertheless, by comparing the $R_p$ values of the mortar specimens exposed to chlorides with those exposed to deionized water, valuable information regarding the passive and active behavior of the rebar can still be obtained. Figure 12 reports $R_p$ vs. time trends for both Slab-A and Slab-B.

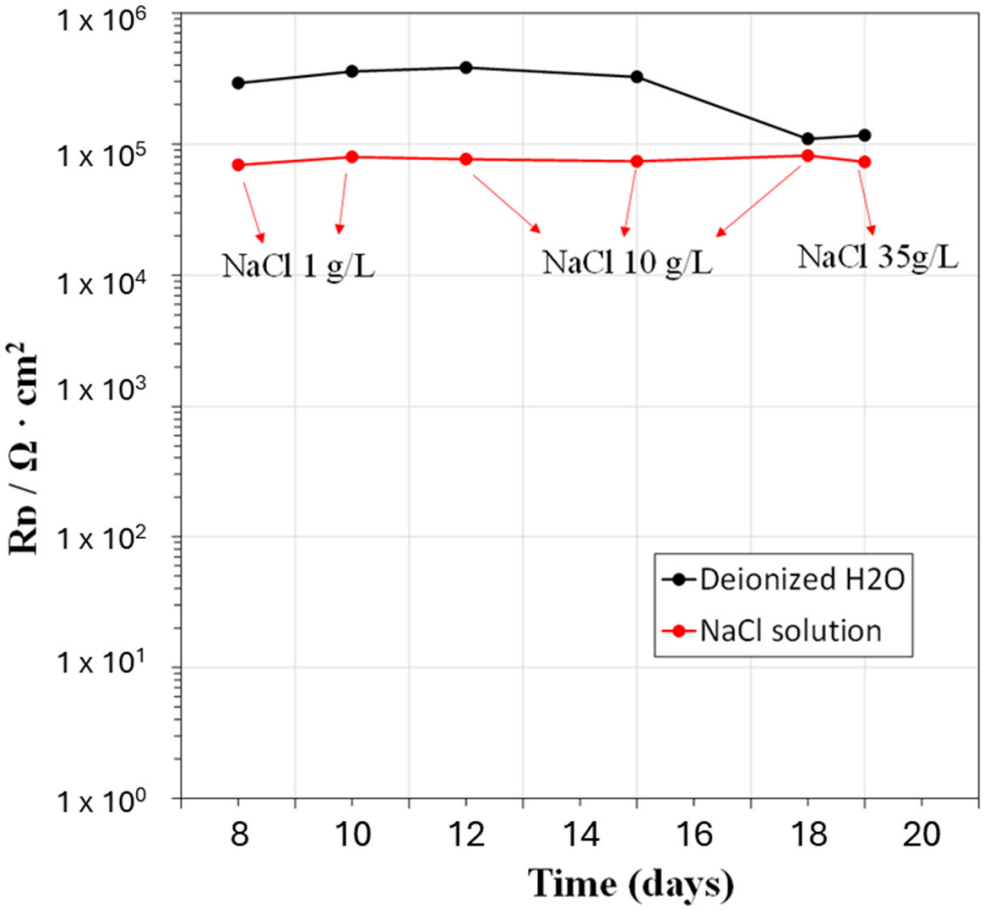



**Figure 12.** $R_p$ vs. time trends recorded during free corrosion on steel-reinforced mortar specimens exposed for 18 days to deionized water, Slab-A (black symbols), and to chloride solutions, Slab-B (red symbols), at different NaCl concentrations (1 g/L, 10 g/L and 35 g/L).

During Phase 2, the rebar of Slab-B exhibited an $R_p$ value of $6.9 \cdot 10^4$ $\Omega \cdot cm^2$, which was about one order of magnitude lower than that ($2.9 \cdot 10^5$ $\Omega \cdot cm^2$) of the Slab-A, exposed to only deionized water. This suggests that chlorides diffused easily through the cement mortar cover (a process also influenced by the specific cement mortar quality used in this study), leading to rebar corrosion. Indeed, $R_p$ values of approximately $7.0 \cdot 10^4$ $\Omega \cdot cm^2$ correspond to a corrosion current density ($i_{cor}$) of about 0.4 $\mu A/cm^2$ (calculated with the Stern–Geary equation $I_{cor} = B/R_p$, assumed to be 26 mVas suggested in the literature for the active corrosion of rebars embedded in mortar [38]). This value exceeds the 0.2 $\mu A/cm^2$ threshold, beyond which is considered to be an active state of corrosion.

Although the chloride concentration was increased to 10 g/L on the tenth day of immersion and to 35 g/L after one week, $R_p$ values remained relatively constant throughout the natural corrosion exposure period. In contrast, Slab-A, only exposed to deionized water, maintained a passive state for about 8 days ($I_{cor}$ around 0.08 μA/cm$^2$). Subsequently, $R_p$ decreased, reaching a value of 1.2·10$^5$ Ω·cm$^2$ ($I_{cor}$ ~ 0.2 μA/cm$^2$) by the end of the exposure. This behavior was likely attributable to cement mortar carbonation.

## 4. Discussion

The effects of reinforcement bar corrosion can be effectively monitored by integrating multiple non-destructive testing (NDT) techniques. In this study, Ground-Penetrating Radar (GPR) and electrochemical methods were employed in combination. The experiments conducted allowed for the identification of variations in the electromagnetic signals that correlate with the electrochemical behavior during the initial stages of rebar corrosion. Specifically, by applying the Hilbert Transform to the A-scans acquired above the reinforcement, a progressive increase in the envelope signal was observed as the corrosion advanced. This variation was also detected during corrosion caused solely by chloride action, i.e., free (natural) corrosion (Figure 8). This aspect highlights the instrument's high sensitivity in identifying an electromagnetic change likely attributed to the production of iron oxides. During the corrosion of the reinforcement bar, iron oxides are formed, which alter the dielectric properties of the mortar surrounding the steel rebar and define a change in the signal reflectivity. Since the beginning of the natural corrosion exposure, the electrochemical measurements ($E_{cor}$ and $R_p$) highlighted values indicative of an active state on the rebar surface. However, these measurements provide information solely about ongoing corrosive processes at the time of measurement. Using Ground-Penetrating Radar (GPR), it is possible to observe the effects of corrosion even if the phenomenon has already occurred, as the electromagnetic signal is altered by the formation of oxides and the modification of the mortar around the reinforcement bar.

Figure 13 presents a diagram in which envelope values obtained by GPR values were correlated with $E_{cor}$ average values measured during the different test conditions. This correlation allows us to understand how the state of corrosion of the sample manifests itself over time and whether this state can be quantitatively defined by the envelope values obtained from the GPR.

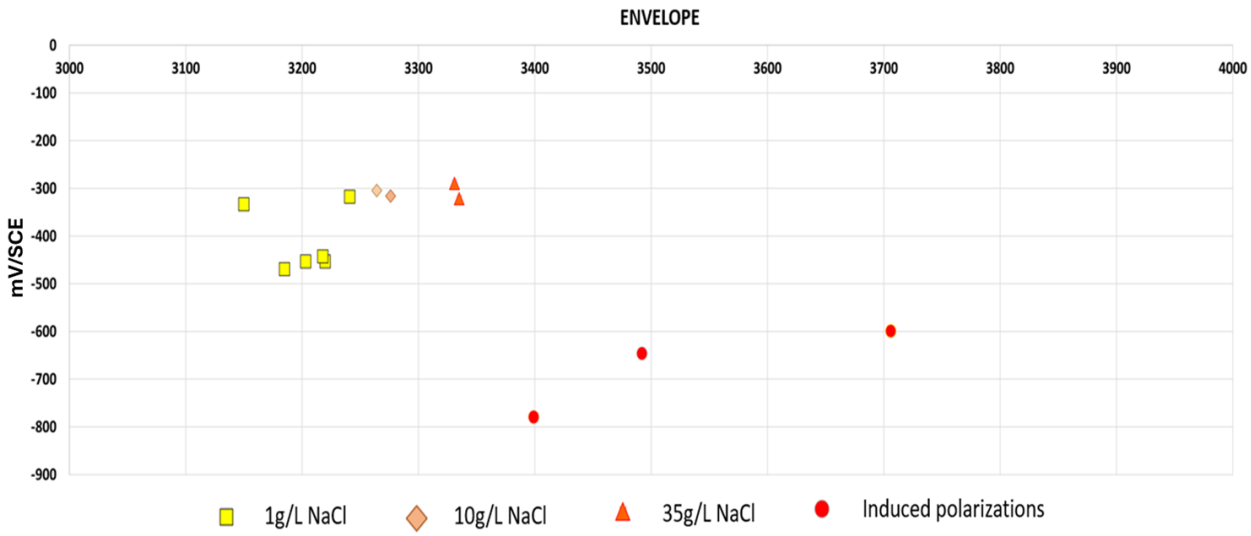



**Figure 13.** Correlation between $E_{cor}$ (mV/SCE) values and the envelope values recorded on Slab-B during free (natural) corrosion and induced polarization phases.

The $E_{cor}$ values reached their lowest values (around −420 mV/SCE) in Phase 1 and then stabilized at around −300 mV/SCE. During this phase, the envelope values depict an increase, rising from around 3150 to around 3325. During the accelerated corrosion phase, while the envelope signal continued to increase from approximately 3400 to 3700, the potential values experienced a strong shift to more negative values (from −800 to −600 mV), potentially resulting from the formation of a thick corrosion-product layer that hinders oxygen diffusion [6]. At the end of the accelerated corrosion tests, Slab-B was opened. As intended, corrosion was mainly localized in the central portion of the steel reinforcement bar. The protected areas were only slightly affected by corrosive phenomena (Figure 14).



**Figure 14.** Slab-B at the end of accelerated corrosion. Corrosion localized in the central portion of the rebar.

The reinforcing bar was extracted from the specimen, and the exposed 8 cm section (previously left uncoated by epoxy resin) was sectioned and cleaned of corrosion products through chemical pickling. By comparing the initial weight of the 8 cm portion of the rebar with the final weight, obtained after chemical pickling, the total mass loss was determined, resulting in a value of 7.5%, confirming a significant reduction in the rebar's cross-sectional area, which can be correlated to the increase in the envelope parameter. These results and the methodological approach adopted in this study provide valuable insights for future investigations aimed at correlating different levels of mass loss with the envelope parameters derived from GPR measurements.

## 5. Conclusions

The rapid urbanization taking place on a global scale necessitates the development of new investigative methodologies that make a significant contribution in terms of time, space, and costs to the characterization and monitoring of existing engineering structures. The main aim is to understand their structural characteristics and degradation, enabling the proper planning of maintenance activities to ensure the durability of the structure and the safety of users. In this context, in addition to traditional diagnostic methodologies, geophysics can provide valuable insights. In order to diagnose the presence of corrosive phenomena in the internal reinforcements of reinforced concrete structures, repeated periodic investigations are necessary, with a focus on monitoring. A single measurement cannot provide information regarding the corrosion status of the reinforcement bars. It should be noted that these investigations can be significantly influenced by various environmental parameters such as humidity and temperature. To determine the possible effects of corrosion, measurements must be carried out using multiple investigative techniques and adopting a multi-sensor approach. The potential method allows for the diagnosis of ongoing corrosion phenomena at the time of measurement. If the reinforcement bar has already been affected by corrosion and there is no longer any activity, no evidence may be detected. By using GPR, we have the ability to diagnose the alteration of the reinforce-

ment bar even if there is no corrosive phenomenon occurring at the time of measurement. The signal variation should be associated with iron oxides and microfractures that occur as the bar corrodes and are retained over time. The result of this research suggests that GPR may enable the detection of reinforcement degradation even when corrosion is not active at the time of the survey. The observed signal variations may be attributed to the presence of iron oxides and the development of micro-cracks, which occur during the corrosion process and persist within the concrete matrix over time. The variations in geophysical parameters could be correlated with the estimation of weight loss in the reinforcement bar. This approach may allow for a quantitative assessment of the reinforcement corrosion phenomenon.

In conclusion, preliminary results are promising; however, establishing a robust correlation between GPR signals and mass loss requires a more extensive dataset. This would provide the necessary calibration to estimate the precise level of corrosion using GPR envelope data. Therefore, future validation must include broader laboratory testing on samples with different characteristics, such as concrete type, rebar size, and concrete cover, utilizing standardized experimental conditions and uniform corrosion parameters to ensure precise calibration. Moreover, future research will focus on testing concrete specimens with varying mass loss to define a precise correlation between reinforcement corrosion and GPR envelope data. Continuing laboratory experiments is crucial to define a standardized procedure that enables the geophysical community working in this field to achieve consistent results.

**Author Contributions:** Conceptualization, E.R. and F.Z.; methodology, E.R., F.Z., and G.F.; software, G.F.; validation, E.R., F.Z., and A.B.; formal analysis, E.R. and F.Z.; investigation, F.G., V.G. and S.R.; resources, E.R. and F.Z.; data curation, G.F.; writing—original draft preparation, E.R., F.Z., and G.F.; writing—review and editing, E.R. and F.Z.; visualization, G.F.; supervision, A.B.; project administration, E.R. and F.Z.; funding acquisition, E.R. and F.Z. All authors have read and agreed to the published version of the manuscript.

**Funding:** This research received no external funding.

**Data Availability Statement:** The original contributions presented in this study are included in the article. Further inquiries can be directed to the corresponding author.

**Conflicts of Interest:** The authors declare no conflicts of interest.

## References

1. Tang, S.W.; Yao, Y.; Andrade, C.; Li, Z.J. Recent Durability Studies on Concrete Structure. *Cem. Concr. Res.* **2015**, *78*, 143–154. [CrossRef]
2. Venkatesan, A.P.; Rajendran, S.; Srinivasan, S.K. Corrosion of Reinforced Concrete Exposed to Marine Atmosfere. *Pdf. Trans. Soc. Adv. Electrochem. Sci. Technol.* **2003**, *38*, 53–56.
3. Pacheco-Torgal, F.; Melchers, R.E.; Shi, X.; De Belie, N.; Van Tittelboom, K.; Perez, A.S. (Eds.) *Eco-Efficient Repair and Rehabilitation of Concrete Infrastructures*, 1st ed.; Woodhead Publishing: Cambridge, UK, 2017; ISBN 9780081021811.
4. Alonso, C.; Andrade, C.; Castellote, M.; Castro, P. Chloride Threshold Values to Depassivate Reinforcing Bars Embedded in a Standardized OPC Mortar. *Cem. Concr. Res.* **2000**, *30*, 1047–1055. [CrossRef]
5. Pacheco Torgal, F.; Miraldo, S.; Labrincha, J.A.; De Brito, J. An Overview on Concrete Carbonation in the Context of Eco-Efficient Construction: Evaluation, Use of SCMs and/or RAC. *Constr. Build. Mater.* **2012**, *36*, 141–150. [CrossRef]
6. Zanotto, F.; Sirico, A.; Balbo, A.; Bernardi, P.; Merchiori, S.; Grassi, V.; Belletti, B.; Malcevschi, A.; Monticelli, C. Study of the Corrosion Behaviour of Reinforcing Bars in Biochar-Added Concrete under Wet and Dry Exposure to Calcium Chloride Solutions. *Constr. Build. Mater.* **2024**, *420*, 135509. [CrossRef]
7. Zanotto, F.; Sirico, A.; Merchiori, S.; Vecchi, F.; Balbo, A.; Bernardi, P.; Belletti, B.; Malcevschi, A.; Grassi, V.; Monticelli, C. Durability of Reinforced Concrete Containing Biochar and Recycled Polymers. *Key Eng. Mater.* **2022**, *919*, 188–196. [CrossRef]
8. Zanotto, F.; Sirico, A.; Balbo, A.; Bernardi, P.; Merchiori, S.; Grassi, V.; Belle, B.; Monticelli, C. Experimental Investigation of Steel Bar Corrosion in Recycled Plastic Aggregate Concrete Exposed to Calcium Chloride Cycles. *Materials* **2025**, *13*, 3361. [CrossRef]

9. Tuutti, K. Corrosion of Steel in Concrete. Ph.D. Thesis, Lund university, Stockholm, Sweden, 1982.
10. Ormellese, M.; Berra, M.; Bolzoni, F.; Pastore, T. Corrosion Inhibitors for Chlorides Induced Corrosion in Reinforced Concrete Structures. *Cem. Concr. Res.* **2006**, *36*, 536–547. [CrossRef]
11. Bossio, A.; Monetta, T.; Bellucci, F.; Lignola, G.P.; Prota, A. Modeling of Concrete Cracking Due to Corrosion Process of Reinforcement Bars. *Cem. Concr. Res.* **2015**, *71*, 78–92. [CrossRef]
12. Daniyal, M.; Akhtar, S. Corrosion Assessment and Control Techniques for Reinforced Concrete Structures: A Review. *J. Build. Pathol. Rehabil.* **2020**, *5*, 1. [CrossRef]
13. Robles, K.P.V.; Yee, J.J.; Kee, S.H. Electrical Resistivity Measurements for Nondestructive Evaluation of Chloride-Induced Deterioration of Reinforced Concrete—A Review. *Materials* **2022**, *15*, 2725. [CrossRef]
14. Ramezanianpour, A.A.; Pilvar, A.; Mahdikhani, M.; Moodi, F. Practical Evaluation of Relationship between Concrete Resistivity, Water Penetration, Rapid Chloride Penetration and Compressive Strength. *Constr. Build. Mater.* **2011**, *25*, 2472–2479. [CrossRef]
15. Boldrin, P.; Fornasari, G.; Rizzo, E. Review of Ground Penetrating Radar Applications for Bridge Infrastructures. *J. Non Destr. Test.* **2024**, *2*, 53–75. [CrossRef]
16. Fornasari, G.; Capozzoli, L.; Rizzo, E. Combined GPR and Self-Potential Techniques for Monitoring Steel Rebar Corrosion in Reinforced Concrete Structures: A Laboratory Study. *Remote Sens.* **2023**, *15*, 2206. [CrossRef]
17. Zaki, A.; Chai, H.K.; Aggelis, D.G.; Alver, N. Non-Destructive Evaluation for Corrosion Monitoring in Concrete: A Review and Capability of Acoustic Emission Technique. *Sensors* **2015**, *15*, 19069–19101. [CrossRef]
18. Tešić, K.; Baričević, A.; Serdar, M. Non-Destructive Corrosion Inspection of Reinforced Concrete Using Ground-Penetrating Radar: A Review. *Materials* **2021**, *14*, 975. [CrossRef] [PubMed]
19. Verma, S.K.; Bhadauria, S.S.; Akhtar, S. Monitoring Corrosion of Steel Bars in Reinforced Concrete Structures. *Sci. World J.* **2014**, *2014*, 957904. [CrossRef]
20. Aperador, W.; Mejía de Gutiérrez, R.; Bastidas, D.M. Steel Corrosion Behaviour in Carbonated Alkali-Activated Slag Concrete. *Corros. Sci.* **2009**, *51*, 2027–2033. [CrossRef]
21. Fornasari, G.; Rizzo, E. A Laboratory Multisensor Geophysical Approach for Monitoring Steel Rebar Corrosion in Concrete Structures. *Bull. Geophys. Oceanogr.* **2024**, *65*, 241–256. [CrossRef]
22. Capozzoli, L.; Rizzo, E. Combined NDT Techniques in Civil Engineering Applications: Laboratory and Real Test. *Constr. Build. Mater.* **2017**, *154*, 1139–1150. [CrossRef]
23. Tosti, F.; Alani, A.M.; Benedetto, A.; Loizos, A.; Soldovieri, F. Guest Editorial: Recent Advances in Non-Destructive Testing Methods. *Surv. Geophys.* **2020**, *41*, 365–369. [CrossRef]
24. Capozzoli, L.; Fornasari, G.; Giampaolo, V.; De Martino, G.; Rizzo, E. Multi-sensors Geophysical Monitoring for Reinforced Concrete Engineering Structures: A Laboratory Test. *Sensors* **2021**, *21*, 5565. [CrossRef]
25. Hong, S.; Lai, W.W.L.; Wilsch, G.; Helmerich, R.; Helmerich, R.; Günther, T.; Wiggenhauser, H. Periodic Mapping of Reinforcement Corrosion in Intrusive Chloride Contaminated Concrete with GPR. *Constr. Build. Mater.* **2014**, *66*, 671–684. [CrossRef]
26. Agred, K.; Klysz, G.; Balayssac, J.P. Location of Reinforcement and Moisture Assessment in Reinforced Concrete with a Double Receiver GPR Antenna. *Constr. Build. Mater.* **2018**, *188*, 1119–1127. [CrossRef]
27. Tesic, K.; Baricevic, A.; Serdar, M.; Gucunski, N. Automation in Construction Characterization of Ground Penetrating Radar Signal during Simulated Corrosion of Concrete Reinforcement. *Autom. Constr.* **2022**, *143*, 104548. [CrossRef]
28. Hubbard, S.S.; Zhang, J.; Monteiro, P.J.M.; Peterson, J.E.; Rubin, Y. Experimental Detection of Reinforcing Bar Corrosion Using Nondestructive Geophysical Techniques. *ACI Mater. J.* **2003**, *100*, 501–510. [CrossRef] [PubMed]
29. Sossa, V.; Pérez-Gracia, V.; González-Drigo, R.; Rasol, M.A. Lab Non Destructive Test to Analyze the E Ff Ect of Corrosion on Ground Penetrating Radar Scans. *Remote Sens.* **2019**, *11*, 2814. [CrossRef]
30. Lai, W.-L.; Kind, T.; Stoppel, M.; Wiggenhauser, H. Measurement of Accelerated Steel Corrosion in Concrete Using Ground-Penetrating Radar and a Modified Half-Cell Potential Method. *J. Infrastruct. Syst.* **2013**, *19*, 205–220. [CrossRef]
31. Shevtsov, D.; Cao, N.L.; Nguyen, V.C.; Nong, Q.Q.; Le, H.Q.; Nguyen, D.A.; Zartsyn, I.; Kozaderov, O. Progress in Sensors for Monitoring Reinforcement Corrosion in Reinforced Concrete Structures—A Review. *Sensors* **2022**, *22*, 3421. [CrossRef]
32. *ASTM C876-91*; Standard Test Method for Half-Cell Potentials of Uncoated Reinforcing Steel in Concrete. ASTM: West Conshohocken, PA, USA, 1999.
33. *ASTM C876-15*; Standard Test Method for Corrosion Potentials of Uncoated Reinforcing Steel in Concrete. ASTM: West Conshohocken, PA, USA, 2015.
34. Hornbostel, K.; Larsen, C.K.; Geiker, M.R. Cement & Concrete Composites Relationship between Concrete Resistivity and Corrosion Rate—A Literature Review. *Cem. Concr. Compos.* **2013**, *39*, 60–72. [CrossRef]
35. Stern, M.; Geary, A.L. Electrochemical Polarization, I. A Theoretical Analysis of the Shape of Polarization Curves. *J. Electrochem. Soc.* **1957**, *104*, 56. [CrossRef]
36. Andrade, C. Propagation of Reinforcement Corrosion: Principles, Testing and Modelling. *Mater. Struct. Constr.* **2019**, *52*, 2. [CrossRef]

37. Sandmeier, K.J. *ReflexW Version 8.1. Program for Processing of Seismic, Acoustic or Electromagnetic Reflection, Refraction and Transmission Data*; Software Manual; Sandmeier Geophysical Research: Karlsruhe, Germany, 2016; 628p.
38. Andrade, C.; Alonso, C. Corrosion Rate Monitoring in the Laboratory and On-Site. *Constr. Build. Mater.* **1996**, *10*, 315–328. [CrossRef]
39. Ahmad, S. Reinforcement Corrosion in Concrete Structures, Its Monitoring and Service Life Prediction—A Review. *Cem. Concr. Compos.* **2003**, *25*, 459–471. [CrossRef]
40. Yuan, Y.; Ji, Y.; Shah, S.P. Comparison of Two Accelerated Corrosion Techniques for Concrete Structures. *ACI Struct. J.* **2007**, *104*, 344–347. [CrossRef] [PubMed]
41. Monticelli, C.; Natali, M.E.; Balbo, A.; Chiavari, C.; Zanotto, F.; Manzi, S.; Bignozzi, M.C. A Study on the Corrosion of Reinforcing Bars in Alkali-Activated Fly Ash Mortars under Wet and Dry Exposures to Chloride Solutions. *Cem. Concr. Res.* **2016**, *87*, 53–63. [CrossRef]
42. Gonzalez, J.A.; Feliú, S.; Andrade, C.; Rodriguez, I. On-Site Detection of Corrosion in Reinforced Concrete Structures. *Mater. Struct. Matrriaux Constr.* **1991**, *24*, 346–350. [CrossRef]

**Disclaimer/Publisher's Note:** The statements, opinions and data contained in all publications are solely those of the individual author(s) and contributor(s) and not of MDPI and/or the editor(s). MDPI and/or the editor(s) disclaim responsibility for any injury to people or property resulting from any ideas, methods, instructions or products referred to in the content.